



**HAL**  
open science

## Integration of ring nanoelectrodes into microwells for the bioelectrochemical analysis in sub-picolitre volumes

Fadhila Sekli-Belaidi, Emilie Vanhove, William Tiddi, Matthieu Polverel, Gabriel Lemercier, Aurélie Lecestre, Jérôme Launay, Pascal Dubreuil, Stéphane Arbault, Pierre Temple-Boyer

### ► To cite this version:

Fadhila Sekli-Belaidi, Emilie Vanhove, William Tiddi, Matthieu Polverel, Gabriel Lemercier, et al.. Integration of ring nanoelectrodes into microwells for the bioelectrochemical analysis in sub-picolitre volumes. *Sensors and Actuators B: Chemical*, 2016, 232, pp.345-356. 10.1016/j.snb.2016.03.130 . hal-01503126

**HAL Id: hal-01503126**

**<https://hal.science/hal-01503126v1>**

Submitted on 6 Apr 2017

**HAL** is a multi-disciplinary open access archive for the deposit and dissemination of scientific research documents, whether they are published or not. The documents may come from teaching and research institutions in France or abroad, or from public or private research centers.

L'archive ouverte pluridisciplinaire **HAL**, est destinée au dépôt et à la diffusion de documents scientifiques de niveau recherche, publiés ou non, émanant des établissements d'enseignement et de recherche français ou étrangers, des laboratoires publics ou privés.

# **Integration of ring nanoelectrodes into microwells for the bioelectrochemical analysis in sub-picolitre volumes**

F. Sékli Belaïdi<sup>1</sup>, E. Vanhove<sup>1</sup>, W. Tiddi<sup>1</sup>, M. Polverel<sup>1</sup>, G. Lemerrier<sup>1</sup>,  
A. Lecestre<sup>1</sup>, P. Dubreuil<sup>1</sup>, J. Launay<sup>1</sup>, S. Arbault<sup>2,3</sup>, P. Temple-Boyer<sup>1</sup>

<sup>1</sup> LAAS-CNRS, Université de Toulouse, CNRS, UPS, Toulouse, France

<sup>2</sup> Université de Bordeaux, ISM, UMR5255, F-33400 Talence, France

<sup>3</sup> CNRS, ISM, UMR5255, F-33400 Talence, France

## **Abstract**

In this work, we report the fabrication and the electrochemical characterization of recessed disk microelectrodes (DME) and ring nanoelectrodes (RNE) integrated in microwell arrays. Such configuration has all advantages of microelectrodes arrays but is more suitable for electrochemical measurement in sub-picolitre volumes (~ 0.3 pL). The technological process based on the reactive ion etching of a SiO<sub>2</sub>/Ti/Pt/Ti/SiO<sub>2</sub> stack is optimized in order to integrate RNE arrays on transparent glass substrate. Multiphysic simulations and electrochemical characterizations are conducted in order to study and improve the amperometric behaviour of recessed ring nanoelectrodes according to their geometry. A good fit is shown between experimental, theoretical and simulation results, allowing full understanding of the electrochemical detection properties of RNE-based microwell arrays. Then, a "generation – collection mode" chronoamperometric approach is proposed to evaluate experimentally the collection ratio of RNE arrays and compare it with simulation results. Finally, first electrochemical characterizations in sub-picolitre volumes are conducted with anti-oxidant species. All these results demonstrate that recessed ring nanoelectrode arrays are fitted to the detection of bio-electrochemical species at the microscale and, consequently to single mitochondrion or single sub-cellular organelle analysis.

**Keywords:** recessed ring nanoelectrode; microwell array; electrochemical characterization; sub-picolitre analysis

**Corresponding author at:** LAAS-CNRS, 7 avenue du colonel Roche, F-31400 Toulouse Cedex 4, France, Tel: +33 561 336 954, Fax: +33 561 336 208, E-mail address: [temple@laas.fr](mailto:temple@laas.fr)

## 1. Introduction

The adaptation of electrochemical detection principles to single cell analysis has increased rapidly in recent years, making them excellent candidates to elucidate the behaviour of different cell secretions [1-4] and powerful tools for diagnosis, therapeutics and drug delivery [5-7]. In the past few decades, rapid monitoring changes in extracellular neuromodulators of many behavioural processes were achieved using ultramicroelectrodes (UME) and/or voltammetric techniques such as amperometry [8-12], fast scan cyclic voltammetry (FSCV) [13-15] and surface modification of electroanalytical probes [16-20]. In the case of retinal cells, amperometry was employed to detect zeptomole quantities of dopamine released upon stimulation [9]. For the study of neurochemical events, FSCV has been employed using microelectrodes arrays (MEA) to image the exocytotic release of dopamine from PC12 cells and to a lesser extent norepinephrine [14]. Other works have shown that the selectivity obtained for Nafion-coated electrodes can be applied for the *in vivo* selective detection of glutamate [17], catecholamine, epinephrine and norepinephrine [16]. Recently, planar microelectrodes integrated into micropits have been used to determine the oxygen consumption activity of mammalian embryos with amperometric measurements [21].

In all cases, single cell analysis has to face two main bottlenecks [22]. The first one is related to cell variability and statistical single-cell multi-analysis. In this context, since glass capillary-based UME were unable to cope with, the development of mass fabrication technologies derived from microelectronics received a great deal of attention. Advances in microfabrication procedures induced new electro-analytical strategies with low-cost fabrication, simple manufacturing, easiness of use and measurement [23-27]. In that way, by developing planar ultra-microelectrode arrays (UMEA), it is possible to perform multi-cell analysis and, consequently, overcome cell variability. Moreover, some works suggested to scale down the dimension of the UME to nanometre size in order to allow their insertion into cells and the final

recording of intracellular signals [28,29]. However, with such approach, it was difficult to avoid cell damages.

From another point of view, the second limitation is associated to the cell-UME spatial configuration impact on electrochemical detection principles. Indeed, whatever the UME type, i.e. glass-capillary-based or planar, electroanalytical recording only partially detects any exocytotic event due to lateral diffusion phenomena promising escapement and loss of an important part of the release [22]. To tackle of this bottleneck, several UMEA have been recently developed to investigate the ability to position a single cell in the UME very close surrounding. This concerns for example the fabrication of microwell arrays with recessed ring micro/nanoelectrodes (RME/RNE), retaining all advantages of UMEA while being better suited for small confined volumes [30,31]. By confining diffusion phenomena and reaching a functional and intricate integration of the "UME-cell" couple, such RNE-based devices will allow, at least, the monitoring of standard cellular metabolisms such as respiration and, at best, the analysis of exocytotic productions. However, up to now, they were not applied to single cell or single sub-cellular organelle analysis due to unsuited dimensions.

In this work, we combine the advantages of microtechnologies with those of reactive ion etching (RIE) technique to fabricate recessed ring nanoelectrodes (RNE) into microwell arrays, aiming to the multi-analysis of single mitochondria. Consequently, we present the microfabrication, modelling/simulation, characterization and application of such electrochemical micro/nanodevices, called ElecWell for electrochemical microwell in this manuscript, for the electrochemical analysis in sub-picolitre volumes ( $\sim 0.3$  pL).

## **2. Experimental section**

### 2.1 Chemical

Methanol ferrocene, potassium chloride, ascorbic acid and dopamine were purchased from

Sigma. Potassium dihydrogenophosphate and di-potassium hydrogenophosphate were purchased from Acros. All reagents were of analytical grade and used as received. The aqueous solutions were prepared with doubled distilled water. High purity nitrogen was used for deaeration.

## 2.2 Electrochemical apparatus

Electrochemical characterization was performed using a three-electrode system with a silver/silver chloride (Ag/AgCl) wire as pseudo-reference electrode and a platinum (Pt) wire as counter electrode. Cyclic voltammetry and chronoamperometry experiments were performed in methanol ferrocene (FcMeOH, 1 mM) and potassium chloride (KCl, 0.1 M) aqueous solutions deaerated with pure nitrogen. For each experiment, a 100 $\mu$ l drop of solution was placed on the studied device using an Eppendorf micropipette. The potentiostat used was a PARSTAT MC (Princeton Applied research) interfaced to a computer, using the VersaStudio software. In all experiments, a low-current amplifier and a Faraday cage were used.

## 2.3 Technological microfabrication

In the frame of the "Electrochemical microwell" (ElecWell) platform, the integration of platinum-based, ring nanoelectrodes (RNE) and disk microelectrodes (DME) into microwell arrays was achieved using silicon-based technologies (figure 1). However, in the frame of single sub-cellular organelle analysis, since transparency will be required to cope finally with optical detection, a transparent B33 glass substrate was chosen. As an option, an initial facultative step consisted in the deposition of a titanium/platinum/titanium (Ti/Pt/Ti, see hereafter) stack patterned using "lift off" technique. This allowed the fabrication of recessed disk microelectrodes (DME) at the microwell bottom in some configurations if necessary (see hereafter). Then, the main technological process involved three deposition steps performed in a row. First, a 2.5  $\mu$ m silicon oxide (SiO<sub>2</sub>) layer was deposited by plasma-enhanced chemical vapour deposition (PECVD). Indeed, compared to polymer-based layers [30], SiO<sub>2</sub> provides

higher dielectric properties, lower electrochemical activities and higher biocompatibility. Then, a 200 nm platinum layer was deposited by evaporation while using two 20nm titanium interfacial layers to ensure platinum adhesion on silicon oxide, and another 2.5  $\mu\text{m}$  PECVD  $\text{SiO}_2$  layer was deposited to form a  $\text{SiO}_2/\text{Ti}/\text{Pt}/\text{Ti}/\text{SiO}_2$  stack. Finally, using a patterned AZ40XT photoresist mask (thickness:  $\sim 13 \mu\text{m}$ ), inductively coupled plasma reactive ion etching (ICP-RIE) was performed and optimized with three different gaseous mixtures (table 1). ICP-RIE process is widely used since it allows an independent control of plasma density and etching ions energy in low-pressure environment. First, silicon oxide  $\text{SiO}_2$  upper layer was etched with a  $\text{CF}_4/\text{Ar}$ -based chemistry, achieving a etch rate and a photoresist selectivity about 150 nm/min and 0.72 respectively. In such a process, argon ions enhance ion bombardment (physical component) while fluorine ions provide chemical reactivity (chemical component), increasing the overall etch rates [32,33]. Furthermore, inert gases are believed to help reducing the re-deposition of micro-masking particles and to remove more effectively any non-volatile residues. In general, it results in smoother etched surfaces with an average surface roughness about 2 nm [34]. The titanium/platinum (Ti/Pt/Ti) layers were then etched using a  $\text{Cl}_2$ -based chemistry (etch rate and photoresist selectivity about 17 nm/min and 0.34 respectively, table 1). Finally, the lower  $\text{SiO}_2$  layer was dry etched using the same  $\text{CF}_4/\text{Ar}$  etching process (as before) in order to reach the B33 glass substrate.

First experiments resulted in microwell arrays with a high roughness bottom that could negatively affect the use of our devices in the frame of optical measurements (figure 2a). This feature was attributed to micromasking phenomena with multiple contributions. First, they should be associated to the deposition of  $\text{CF}_x$  complexes on microwell surfaces. Second, they should be related to the physical bombardment by argon ions, responsible for the break of Si-O bonds, which results in the release of oxygen atoms in gaseous phase and, consequently, in the formation of titanium oxides ( $\text{TiO}_x$ ) at the  $\text{SiO}_2$  etch end. Globally, both thin  $\text{CF}_x$  and/or  $\text{TiO}_x$ -based barrier layers can act as micromasks due to local differences of etch rates during the

CF<sub>4</sub>/Ar RIE process. Thus, the micro-masking residues can interfere with proper etching of the underlying silicon oxide layers, creating undesirable "fairy-chimney" microstructures (figure 2b). Methods for preventing the formation of micromasking residues include the use of chemically reactive agents for isotropic attack in order to loose cones from their weakened bases without causing excessive damage to underlying layers. SF<sub>6</sub>-based chemistry was therefore added to remove the barrier layers from the surface before and after platinum etching [35]. According to the experimental conditions used (table 1), results from SF<sub>6</sub> plasma treatment support this assertion since the SF<sub>6</sub> etch step (duration: 3 minutes) prevented from any micromasking phenomena, leading to smooth surface at the microwell bottom (figures 2c and 2d).

Furthermore, since the second CF<sub>4</sub>/Ar etching process is not fully anisotropic, the upper SiO<sub>2</sub> layer is over-etched during the lower SiO<sub>2</sub> layer etching, leading to the creation of a step (width  $L$ ) on the platinum layer that forms the ring nanoelectrode (figure 3a). This step width  $L$  was found to be a function of the SiO<sub>2</sub> lower layer thickness. It was estimated experimentally to be roughly equal to  $0.12 H_l$ , i.e. around  $0.3 \mu\text{m}$  (figure 3b).

All in all, after optimizing the etching process for the whole SiO<sub>2</sub>/Ti/Pt/Ti/SiO<sub>2</sub> stack, we were able to mass fabricate effectively recessed ring nanoelectrodes (RNE) into microwell arrays and associated ElecWell electrochemical nanodevices on transparent B33 glass substrate (figure 4). Three different configurations were realized on chip, leading to the fabrication of  $1 \times 1$ ,  $10 \times 10$  and  $100 \times 100$  microwell arrays with integrated RNE nanodevices. On the one side, the two largest designs ( $10 \times 10$  and  $100 \times 100$ ) are planned to perform parallel measurement in order to increase measured current (cf. microelectrode array theory), to overcome cell variability thanks to averaging methods, and/or to reach statistical analysis of single mitochondria. On the other side, according to the mitochondrial filling rate of microwells, the two smallest designs ( $1 \times 1$  and  $10 \times 10$ ) are planned to compete with the single mitochondrion analysis in sub-picolitre volume.

### 3. Results and discussion

The Elecwell configuration could be developed for different applications such as bio-electrochemical detection at the micro- or even nano-scale [30,31] or single cell analysis. In the second cases, studies have to take into account the size of the biological entity of interest. Following previous ones [26], these works and associated realisations are dedicated to the single mitochondrion analysis and, consequently, concern the integration of microwells in the [1 – 10  $\mu\text{m}$ ] range.

#### 3.1 Design optimization of ring nanoelectrodes integrated into microwells

The integration of ring nanoelectrodes (RNE) into microwells was studied and optimized by multiphysic simulation. In fact, it was necessary to model the diffusion and collection phenomena inside the microwell and to evaluate the best approach to enhance the electrochemical signal. The lower  $\text{SiO}_2$  layer thickness ( $H_I$ ) determines the vertical distance between the microwell bottom where the emission takes place (inflow definition) and the ring nanoelectrode where the collection occurs (outflow determination). The microwell inner radius ( $R$ ) plays a role on diffusion profiles. A crude example will be seen for the platinum electrode thickness ( $T$ ) since its increase improves the collection factor. All these parameters had to be taken into account and cross-related during simulation to save time and technological resources for fabricating already optimized designs. For our study, diffusion phenomena in a microwell were simulated using the commercial software COMSOL Multiphysics 4.3 in order to find the optimal geometry for the ring nanoelectrodes into microwell design. A 2D axisymmetric model was used in the simulation as illustrated in figure 5.

The *Transport of Diluted Species* (chds) module takes into account the convection, migration and diffusion equations. In our model, only the third element will have a non-zero contribution

since neither electric field nor stirring are applied to the solution. Since only diffusion phenomena take place, Fick's laws give the resulting differential equations:

$$\frac{\partial C_i}{\partial t} + \nabla(-D_i \nabla C_i) = R_i \quad (1)$$

$$N_i = -D_i \nabla C_i \quad (2)$$

where  $C_i$  represents the concentration of the studied species ( $\text{mol m}^{-3}$ ),  $D_i$  its diffusion coefficient ( $\text{m}^2 \text{s}^{-1}$ ),  $R_i$  the rate of eventual reactions taking place consuming or producing the species ( $\text{mol m}^{-3} \text{s}^{-1}$ ) and  $N_i$  the diffusion flux across the electrode surface ( $\text{mol m}^{-2} \text{s}^{-1}$ ).

The parameter of interest for the simulation will be the collection ratio, defined as the ratio between the outflow (flow of species reacting on the ring nanoelectrode) and the inflow (flow of species generated at the microelectrode bottom). This will give information concerning the confinement/entrapment of released species in order to enhance detection performances. The effects of the total height ( $H = H_1 + T + H_2$ ) and radius ( $R$ ) on the collection ratio were studied for different emission radii ( $M$  ranging between  $1 \mu\text{m}$  and  $6 \mu\text{m}$ ). The results are shown in figures 6a and 6b. They are intertwined since both are related to a more general concept, the aspect ratio  $H/R$ . The higher it is, the narrower is the well, and, consequently, the better is the confinement as well as the associated collection ratio.

Since the collection ratio is increasing with the aspect ratio  $H/R$ , optimization will be finally obtained for the highest height  $H$  and for the lowest radius  $R$ . Nevertheless, for technological reasons associated to the AZ40XT photoresist resolution and etch during the different ICP-RIE processes (see table 1: selectivity values), it was difficult to obtain microwell radii lower than  $3 \mu\text{m}$  and depths higher than  $5 \mu\text{m}$ . As a result, the microwell geometry was chosen at best to be  $5 \mu\text{m}$  in depth and  $3$  or  $4.5 \mu\text{m}$  in radius.

The ring nanoelectrode thickness  $T$  deserves a specific mention. As can be seen in figure 6c, the ideal and logical pattern would be to increase its value in order to achieve a wider area of

depletion around it, improving the collection factor. Even if simulation shows useful gain with its increment, it has forcefully been limited at about 200 nm for technological reasons, i.e. low stress phenomena and good adhesion properties into the SiO<sub>2</sub>/Ti/Pt/Ti/SiO<sub>2</sub> stack.

Next parameter of interest is the height of the electrode within the well  $H_1$ , recognizable also as the thickness of the lower SiO<sub>2</sub> layer. Contrary to previous graphs, the curves show a non-monotonic behaviour characterized by an  $M$ -dependent optimum (figure 6d). This is due to a competition between two phenomena: on one side approaching the electrode towards the bottom produces stronger gradient due to small distance between the released species and the diffusion layer of electrode, on the other side getting too close affects the solid angle overlay between emission and collection. From our results, it is better to locate the ring nanoelectrode at the microwell mid-height and therefore, according to previous considerations, to choose a value around 2.5  $\mu\text{m}$  that is not far from higher optima.

Finally, even it is a technological-related parameter, it was opportune to examine the influence of the step width  $L$  on the collection ratio. Indeed, this geometric parameter may have contradictory effects. On the one hand, the formed step offers more electroactive surface and increases the collected current on the ring nanoelectrode. On the other hand, the over-etch of the SiO<sub>2</sub> upper layer increases the microwell radius and reduces the  $H/R$  aspect ratio. Consequently, the  $L$  value was varied between 0 to 0.5  $\mu\text{m}$  when keeping the other parameters constant. Regardless the microwell radius, the higher collections ratios were achieved for the wider step (table 2). Nevertheless, main collection ratio increases were obtained in the [0 – 0.3  $\mu\text{m}$ ] range. For a 3 $\mu\text{m}$  radius, the presence of the 0.3 $\mu\text{m}$ -wide step (as revealed by SEM observations) achieves a collection ratio improvement from 78 to 83.3%. For a 4.5  $\mu\text{m}$  radius, the improvement goes from 70.4 to 76.7%. Beyond 0.3  $\mu\text{m}$ , the gain becomes less significant due to a saturation effect (table 2). This is explained by the fact that, when  $R$  increases, the microwell is less narrow and fewer species are confined.

So, the ElecWell technological process described above adopted the following geometrical

parameters (that will be retained hereafter): microwell radius  $R$  of 3 and 4.5  $\mu\text{m}$ , lower and upper  $\text{SiO}_2$  layer thicknesses  $H_1$  and  $H_2$ :  $\sim 2.5 \mu\text{m}$ , step width  $L$ :  $\sim 0.3 \mu\text{m}$ , ring nanoelectrode thickness  $T$ :  $\sim 0.2 \mu\text{m}$ , microwell total height  $H$  around 5.2  $\mu\text{m}$ .

### 3.2 Electrochemical characteristics of recessed disk microelectrodes (DME) and ring nanoelectrodes (RNE)

The different ElecWell electrochemical devices were finally characterized by cyclic voltammetry (CV) in order to validate their electrochemical behaviour and to study their potentiality towards sub-picolitre analysis. Figures 7a and 7b show the voltammetric responses at different scan rates (from 5 to 500 mV/s) of DME and RNE in aqueous solution containing 1 mM Fc(MeOH) and 0.1 M KCl respectively. In the first case (figure 7a), CV measurements produce a transient response with a slow decay of the faradaic current plateau. Surprisingly, limiting currents were found to depend slightly on the scan rate (a phenomenon currently under investigation). Nevertheless, at the slowest scan rate (5 mV/s), a steady-state response with limiting current of 230 pA was observed. This behaviour is in good agreement with theoretical studies associated to recessed disk microelectrodes [36,37]. According to equation (3) and considering an average radius of 3  $\mu\text{m}$  and a recessed depth of 5.2 $\mu\text{m}$ , a limiting current of 221 pA was estimated.

$$I_{lim} = \frac{4nFD_{diff}CR}{1 + \frac{4H}{\pi R}} \quad (3)$$

where  $n$  is the number of electrons transferred ( $n = 1$ ),  $F$  is the Faraday constant ( $F = 96485 \text{ C mol}^{-1}$ ),  $D_{diff}$  is the Fc(MeOH) diffusion coefficient ( $D_{diff} = 6.1 \times 10^{-6} \text{ cm}^2/\text{s}$  in 0.1 M KCl),  $C$  is the bulk concentration ( $C = 10^{-3} \text{ mol/L}$ ),  $H$  is the disk microelectrode recessed depth ( $H = 5.2 \mu\text{m}$ ), and  $R$  is the disk microelectrode radius ( $R = 3 \mu\text{m}$ ).

The same behaviour was observed with recessed ring nanoelectrodes: a steady-state

sigmoidal response with slight hysteresis on the reverse scan was therefore achieved (figure 7b). Similar to the microdisk responses, the limiting currents of the recessed nanoring electrodes were slightly depending on the scan rates. It was noted that a range of 400-448 pA was measured while scan rates varied between 5 and 500 mV/s. In the literature, few studies have been devoted to examine the electrochemical responses of planar ring microelectrodes compared to planar disk microelectrodes that attract wide attention. Recessed ring nanoelectrodes were commonly used in generator-collector experiments [38,39] and only the expression of microdisk limiting current was reported in most cases. Recently, L. Zhuang et al. tried to correlate the limiting current of recessed nanoring with the equation of recessed microdisk [40]. The discrepancy between the experimental and theoretical currents was reported to be associated with the edge effects that enhance the electrode signal. To the best of our knowledge, no theoretical investigation was performed to study the diffusion process at recessed ring microelectrode. Therefore, from Szabo works [41] that describe the limiting current of ring nanoelectrodes, we have developed a mathematical model that describes the expression of the current at stationary domain:

$$I_{lim} = \frac{nFD_{diff}CL_0}{1 + \frac{4H_2}{\pi(R+L)}} \quad (4)$$

with:

$$L_0 = \frac{\pi^2(2R+L)}{\ln\left(\frac{32R}{L} + \exp\left(\frac{\pi^2}{4}\right)\right)} \quad (5)$$

where  $n$  is the number of electrons transferred ( $n = 1$ ),  $F$  is the Faraday constant ( $F = 96485 \text{ C mol}^{-1}$ ),  $D_{diff}$  is the Fc(MeOH) diffusion coefficient ( $D_{diff} = 6.1 \times 10^{-6} \text{ cm}^2/\text{s}$  in 0.1 M KCl),  $C$  is the bulk concentration ( $C = 10^{-3} \text{ mol/L}$ ), the length  $l_0$  depends on the ring nanoelectrode geometry,  $H_2$  is the ring nanoelectrode recessed depth ( $H_2 = 2.5 \text{ }\mu\text{m}$ ),  $R$  is the microwell inner radius ( $R = 3 \text{ }\mu\text{m}$ ) and  $L$  is the step width ( $L = 0.3 \text{ }\mu\text{m}$ ).

Considering experimental values of limiting current  $I_{lim}$  estimated at slow scan rate (5 mV/s), a good fit was obtained with mathematical equations (4) and (5) as well as COMSOL simulation, validating our theoretical model (table 3).

### 3.3 Electrochemical investigations of recessed ring nanoelectrode arrays

The microwell centre-to-centre distance  $D$  between neighbouring microelectrodes in MEA is a key factor since it significantly affects the electrochemical response of the arrays. To obtain a steady state conditions,  $D$  must be sufficiently large to avoid diffusion layers overlapping [42,43]. Therefore, we investigated the electrochemical behaviours of the recessed ring nanoelectrode (RNE) microwell arrays by measuring voltammetric responses for different  $D/R$  ratios in order to define the smallest  $D$  value that prevents diffusion layers overlapping.

The scan rate studies were performed for  $10 \times 10$ , 3  $\mu\text{m}$ -radius, RNE arrays by measuring voltammetric responses for different  $D/R$  ratios and scan rates varying between 5 and 500 mV/s. Thus, we should identify experimentally the necessary  $D$  that is large enough to allow the development of hemispherical diffusion layers over the individual microelectrode in the array. Cyclic voltammograms (CV) of the recessed RNE arrays ( $R = 3 \mu\text{m}$ ) in 1 mM Fc(MeOH) are shown in figures 8a and 8b. It can be seen that when  $D$  equals  $5R$  (Figure 8a), the RNE array response loses the steady state characteristic, indicating consequent overlapping of individual diffusion layers associated to adjacent microelectrodes and the development of planar diffusion. In this case, mass transport to the electrodes was reduced and measured current was lower in comparison to its theoretical values. Upon increasing the  $D/R$  ratio, current responses switch between planar and hemispherical diffusion. When the RNE were well separated ( $D = 20R$ ) (Figure 8b), steady state behaviour was obtained when scan rate varied from 50 to 500 mV/s.

As we decrease the scan rate, the timescale of the experiment increases resulting in larger diffusion zones and a current decrease. On the other hand, if we increase scan rate, we shorten the timescale of the experiment resulting in smaller diffusion zones. Thus, we can usually avoid

overlapping and move from planar to hemispherical diffusion by simply increasing the scan rate. From our results, a clear conclusion is that an optimized centre-to centre-distance of  $20R$  was necessary to avoid diffusion layers overlapping and to allow steady state characteristics even for the lowest scan rates. This design rule was retained for the ElecWell platform and kept for the following studies.

### 3.4 Electrochemical characterization of the DME – RNE electrochemical system in generator-collector mode

In order to check the confinement effects of microcavities on the amperometric responses, we investigate the electrochemical behaviour of the  $10 \times 10, 3 \mu\text{m}$ -radius, RNE arrays ( $D = 20R$ ) in generator/collector working mode. Microwells used in this study contain recessed disk microelectrodes (DME) at their bottom and recessed ring nanoelectrodes (RNE) at their mid-depth. In the present experiment, the disk microelectrode was held at an anodic potential ( $E = 0.4 \text{ V}$  versus Ag/AgCl) in order to oxidize ferrocene (Fc) to ferrocenium ( $\text{Fc}^+$ ). Then,  $\text{Fc}^+$  species were reduced on the ring nanoelectrodes held at a cathodic potential ( $E = 0 \text{ V}$  versus Ag/AgCl). Finally, the regenerated Fc species can diffuse back to the disk electrodes for re-oxidation.

Typical chronoamperometric curves obtained for disk microelectrodes and ring nanoelectrodes are presented on figure 9. In both cases, steady-state responses were clearly demonstrated, allowing the limiting current measurement. First, the DME limiting current values were compared for RNE nanodevices polarized or not. Thus, an amplification ratio around 130% was calculated to characterize the generator-collector mode. Then, the ratio between the RNE and DME limiting currents yielded a collection factor around 76%. This result is consistent with the previous COMSOL simulations (table 2) that have predicted a collection ratio around 83% for the studied electrochemical system. Such discrepancy between experiment and simulation should be associated to approximations on the effective geometrical parameters, and especially on the inner radius  $R$ , the step width  $L$  and the ring nanoelectrode thickness  $T$ .

### 3.5 Electrochemical analysis of dopamine in presence of ascorbic acid using the DME – RNE system

In vivo measurements with interfering molecules others than those of interest are often limited by the resolution of redox phenomena. The recessed disk/ring electrodes into microwells can experimentally be used to decrease effectively overlaps between diffusion waves. In order to do so, the ring nanoelectrode potential should be fixed at the unwanted redox wave while the disk microelectrode potential is scanned across the wave associated to the analyte of interest. Under such conditions, most of the interfering species are consumed at the ring nanoelectrode and cannot access to the disk microelectrode at the bottom of the microwell. This phenomenon was studied by using solutions of ascorbic acid (AA) and dopamine (Dop) as a model. Such detection is of particular interest owing to the biological importance of these analytes. In previous works, we had used PEDOT surface modification to assay them selectively in presence of uric acid [44,45]. Here, we used microwells recessed disk/ring electrodes to decrease the redox interference.

For the first experiment, when the ring nanoelectrode was not polarized, the voltammogram obtained for AA and Dop mixture on disk microelectrode showed a broad anodic current (figure 10). Two overlapped waves were present with half-wave potentials  $E_{1/2}$  close to 0.3 V and 0.5 V for AA and Dop respectively with a plateau current in the range of dopamine wave. These results are in agreement with previous works, demonstrating if necessary the measurement interferences between AA and Dop species on metallic electrodes [25,44]. For the second experiment, the disk microelectrode was scanned in the same conditions whereas the ring nanoelectrode was held at 0.3 V to oxidize ascorbic acid and avoid his presence close to disk microelectrode. Interestingly, the CV wave behaves as a pure diffusional one similar to that observed for dopamine investigated alone (third experiment).

The above results demonstrate that the DME-RNE system is able to address problems

associated to electroanalytical selectivity. In order to analyse quantitatively the interference reducing effect, simulations were performed using the DME-RNE model developed using COMSOL Multiphysics 4.3. According to our simulation results (table 4), it appears that the selectivity ratio increases with the microwell radius decrease. Nevertheless, the associated reducing interference effect appears to be effective only for  $[AA]/[Dop]$  ratios lower than 10. For comparison, a configuration including a top plane electrode all around the recessed DME microwell array (as proposed by A. Oleinick et al. [45]) was also simulated, evidencing improved results but similar limitations in term of selectivity (table 4). As a matter of fact, it should be concluded that the DME-RNE system can address electroanalytical selectivity problems but is not adapted to the detection of dopamine in presence of ascorbic acid in the frame of blood analysis ( $[AA]/[Dop] > 10$  [46,47]).

#### 4. Conclusion

Microwell arrays with platinum-based, recessed ring nanoelectrodes (RNE) were successfully integrated, studied and optimized for the electrochemical analysis in sub-picolitre volumes ( $\sim 0.3$  pL). The associated microfabrication process is based on the reactive ion etching of a  $\text{SiO}_2/\text{Ti}/\text{Pt}/\text{Ti}/\text{SiO}_2$  stack integrated on a transparent glass substrate. The main technological bottleneck encountered was associated with micromasking phenomena due to the formation of  $\text{CF}_x$  and/or  $\text{TiO}_x$ -based complexes. It was finally solved thanks to the use of a dedicated  $\text{SF}_6$  etch step. Multiphysic simulations were conducted in order to study the global behaviour of recessed ring nanoelectrodes according to their geometry. It was found that the higher collection ratios were obtained for the higher microwell aspect ratio  $H/R$ , the thicker platinum layer (thickness  $T$ ) and a nanoelectrode location around the microwell mid-height ( $H_1 = H_2$ ). Thus, taking into account technological constraints as well as exploiting over-etch phenomenon of the upper  $\text{SiO}_2$  layer, recessed ring nanoelectrode were successfully microfabricated with the following

parameters: radius microwell between 3 and 4.5  $\mu\text{m}$ ,  $\text{SiO}_2$  layer thickness:  $\sim 2.5 \mu\text{m}$ , 200nm-thin ring nanoelectrode located at the microwell mid-height, microwell total height around 5.2  $\mu\text{m}$ .

Electrochemical characterizations were then performed in order to study the amperometric behaviour of recessed ring nanoelectrodes. Using cyclic voltammetry, a good fit was demonstrated between experimental, theoretical and simulation results. This was extended to RNE microwell arrays, showing that a ratio of 20 between microwell centre-to-centre distance and radius was necessary to avoid diffusion layers overlapping and to ensure steady state characteristics regardless of the scan rate. Then, a "generation – collection mode" chronoamperometric approach was proposed using microwell arrays with both recessed disk microelectrodes (DME) at their bottom and recessed ring nanoelectrodes (RNE) at their mid-depth. Thus, the amplification ratio into the microwell and the collection ratio between RNE and DME devices were respectively estimated to 130% and 76%, in agreement with multiphysic simulations. Finally, first cyclic voltammetric characterizations in sub-picolitre volumes were conducted for the analysis of anti-oxidant species and more especially the detection of dopamine in presence of ascorbic acid, demonstrating the potentiality of the DME – RNE system to address electroanalytical selectivity problems for concentration ratios lower than 10.

All these results demonstrate that recessed ring nanoelectrode (RNE) arrays are well fitted for the electrochemical detection of biochemical species at the microscale or even nanoscale and, consequently, for the analysis of single sub-cellular organelles such as mitochondria. The use of a transparent glass substrate is in this case mandatory since, apart from electrochemical micro-analysis considerations, optical measurements are required in order to check the effective presence of a mitochondrion into the microwell or even to perform some optical-based analysis (e.g. fluorescence,...). In this context, the use of RNE-based devices will allow different approaches to study mitochondrial metabolisms associated to respiration ( $\text{O}_2$  detection) as well as to the production of hydrogen peroxide ( $\text{H}_2\text{O}_2$ ) and other reactive oxygen species (ROS). First, RNE arrays will be used in order to analyse several single mitochondria while increasing

the measured current (cf. microelectrode array theory) and dealing with biological variability thanks to averaging methods. Then, RNE array size will be decreased as much as possible in order to perform a single mitochondrion analysis. Finally, array of independent RNE devices will be developed in order to reach statistical analysis and to overcome fully biological variability.

## Acknowledgements

The authors would like to thank the French "Agence nationale de la Recherche" (ANR, project NANOMITO, n° ANR-2011-BSV-502501). Furthermore, the technological realisations and associated research works were partly supported by the French RENATECH network.

## References

- [1] R.A. Clark and A.G. Ewing, A.G., "Quantitative measurement of released amines from individual exocytotic events", *Molecular Neurobiology*, 15 (1997) 1–16
- [2] R.M. Wightman, "Probing cellular chemistry in biological systems with microelectrodes", *Science*, 311 (2006) 1570–1574
- [3] C. Amatore, S. Arbault, M. Guille and F. Lemaitre, "Electrochemical monitoring of single cell secretion: vesicular exocytosis and oxidative stress", *Chemical Review*, 108 (2008) 2585-2621
- [4] A.G. Ewing, J.C. Bigelow and R.M. Wightman, "Direct in vivo monitoring of dopamine released from two striatal compartments in the rat", *Science*, 221 (1983) 169-171
- [5] A. Lad and Y.K. Agrawal, "Nanodevices for monitoring toxicological behavior of therapeutic agent", *Review in Nanoscience and Nanotechnology*, 1 (2012) 217-227
- [6] M. Mazloun-Ardakani, L. Hosseinzadeh and A. Khoshroo, "Label-free electrochemical immunosensor for detection of tumor necrosis factor  $\alpha$  based on fullerene-functionalized carbon nanotubes/ ionic liquid", *Journal of Electroanalytical Chemistry*, 757 (2015) 58-64

- [7] P. Duangkaew, S. Tapaneeyakorn, C. Apiwat, T. Dharakul, S. Laiwejpithaya, P. Kanatharana and R. Laocharoensuk, "Ultrasensitive electrochemical immunosensor based on dual signal amplification process for p16(INK4a) cervical cancer detection in clinical samples", *Biosensors & Bioelectronics*, 74 (2015) 673-679
- [8] J.M. Finnegan, K. Pihel, P.S. Cahill, L. Huang, S.E. Zerby, A.G. Ewing, R.T. Kennedy and R.M. Wightman, "Vesicular quantal size measured by amperometry at chromaffin, mast, pheochromocytoma and pancreatic cells", *Journal of Neurochemistry*, 66 (1996) 1914–1923
- [9] S.E. Hochstetler, M. Puopolo, S. Gustincich, E. Raviola and R.M. Wightman, "Real-time amperometric measurements of zeptomole quantities of dopamine released from neurons", *Analytical Chemistry*, 72 (2000) 489-496
- [10] C. Amatore, S. Arbault and A.C.W. Koh, "Simultaneous detection of reactive oxygen and nitrogen species released by a single macrophage by triple potential-step chronoamperometry", *Analytical Chemistry*, 82 (2010) 1411-1419
- [11] X. Liu, S. Barizuddin, W. Shin, C.J. Mathai, S. Gangopadhyay and K.D. Gillis, "Microwell device for targeting single cells to electrochemical microelectrodes for high-throughput amperometric detection of quantal exocytosis", *Analytical Chemistry*, 83 (2011) 2445-2451
- [12] Y.S. Song and S. Bai, "Characterization of a single cell of *Chlorella* in a microfluidic channel using amperometric electrode arrays", *Biotechnology Letters*, 36 (2014) 2185-2191
- [13] J.J. Day, M.F. Roitman, R.M. Wightman and R.M. Carelli, "Associative learning mediates dynamic shifts in dopamine signaling in the nucleus accumbens", *Nature Neuroscience*, 10 (2007) 1020-1028
- [14] B. Zhang, K.L. Adams, S.J. Lubner, D.J. Eves, M.L. Heien and A.G. Ewing, "Spatially and temporally resolved single-cell exocytosis utilizing individually addressable carbon microelectrode arrays", *Analytical Chemistry*, 80 (2008) 1394–1400

- [15] A.R. Smith, P.A. Garris, and J.M. Castro, "Real-time monitoring of electrically evoked catecholamine signals in the songbird striatum using in vivo fast-scan cyclic voltammetry", *Journal of Chemical Neuroanatomy*, 66-67 (2015) 28-39
- [16] D.J. Leszczyszyn, J.A. Jankowski, O.H. Viveros, E.J. Diliberto, J.A. Near and R.M. Wightman, "Secretion of catecholamines from individual adrenal medullary chromaffin cells", *Journal of Neurochemistry*, 56 (1991) 1855-1863
- [17] N.V. Kulagina, L. Shankar and A.C. Michael, "Monitoring glutamate and ascorbate in the extracellular space of brain tissue with electrochemical microsensors", *Analytical Chemistry*, 71 (1999) 5093-5100
- [18] H.G. Sudibya, J.M. Ma, X.C. Dong, S. Ng, L.J. Li, X.W. Liu and P. Chen, "Interfacing glycosylated carbon nanotube network devices with living cells to detect dynamic secretion of biomolecules", *Angewandte Chemie*, 48 (2009) 2723–2726
- [19] S.Y. Yang, B.N. Kim, A.A. Zakhidov, P.G. Taylor, J.K. Lee, C.K. Ober, M. Lindau and G.G. Malliaras, "Detection of transmitter release from single living cells using conducting polymer microelectrodes", *Advanced Materials*, 23 (2011) H184–H188
- [20] B.X. Shi, Y. Wang, K. Zhang, T.L. Lam and H.L. Chan, "Monitoring of dopamine release in single cell using ultrasensitive ITO microsensors modified with carbon nanotubes", *Biosensors & Bioelectronics*, 26 (2011) 2917–2921
- [21] Y. Date, S. Takano, H. Shiku, K. Ino, T. Ito-Sasaki, M. Yokoo, H. Abe and T. Matsue, "Monitoring oxygen consumption of single mouse embryos using an integrated electrochemical microdevice", *Biosensors & Bioelectronics*, 30 (2011) 100-106
- [22] C. Amatore, J. Delacotte, M. Guille-Collignon and F. Lemaître, "Vesicular exocytosis and microdevices – microelectrodes arrays", *Analyst*, 140 (2015) 3687-3695
- [23] D. Quinton, A. Girard, L.T.T. Kim, V. Raimbault, L. Griscom, F. Razan, S. Griveau and F. Bedioui, "On-chip multi-electrochemical sensor array platform for simultaneous screening of nitric oxide and peroxynitrite", *Lab on Chip*, 11 (2011) 1342-1350

- [24] Y. Temiz, A. Ferretti, Y. Leblecici and C. Guiducci, "A comparative study on fabrication techniques for on-chip microelectrodes", *Lab on Chip*, 12 (2012) 4920-4928
- [25] C. Christophe, F. Sékli Belaidi, J. Launay, P. Gros, E. Questel and P. Temple-Boyer, "Elaboration of integrated microelectrodes for the detection of antioxidant species", *Sensors & Actuators B*, 177 (2013) 350–356
- [26] S. Ben Amor, E. Vanhove, F. Sékli Belaidi, S. Charlot, D. Colin, M. Rigoulet, A. Devin, J. Launay, P. Temple-Boyer and S. Arbault: "Enhanced detection of hydrogen peroxide with platinumized microelectrode arrays for analyses of mitochondria activities", *Electrochimica Acta*, 126 (2014) 171-178
- [27] A. Weltin, K. Slotvinski, J. Kieninger, I. Moser, G. Jobst, M. Vego, R. Ehret and G.A. Urban: "Cell culture monitoring for drug screening and cancer research: a transparent, microfluidic, multi-sensor microsystem", *Lab on Chip*, 14 (2014) 138-146
- [28] P. Sun, F.O. Laforge, T.P. Abeyweera, S.A. Rotenberg, J. Carpino and M.V. Mirkin, "Nanoelectrochemistry of mammalian cells", *Proceedings of the National Academy of Science of the USA*, 105 (2008) 443-448
- [29] Y.X. Wang, J.M. Noel, J. Velmurugan, W. Nogala, M.V. Mirkin, C. Lu, M.G. Collignon, F. Lemaitre and C. Amatore, "Nanoelectrodes for determination of reactive oxygen and nitrogen species inside murine macrophages", *Proceedings of the National Academy of Science of the USA*, 109 (2012) 11534-11539
- [30] Z.P. Aguilar, W.R. Vandaveer and I. Fritsch, "Self-contained microelectrochemical immunoassay for small volumes using mouse IgG as a model system", *Analytical Chemistry*, 74 (2002) 3321-3329
- [31] C. Ma, N.M. Contento, L.R. Gibson and P.W. Bohn, "Redox cycling in nanoscale-recessed ring-disk electrode arrays for enhanced electrochemical sensitivity", *ACS Nano*, 7 (2013) 5483-5490

- [32] L. Li, T. Abe and M. Esashi, "Smooth surface glass etching by deep reactive ion etching with SF<sub>6</sub> and Xe gases", *Journal of Vacuum Science and Technology*, 21 (2003) 2545-2549
- [33] J.H. Park, N.E. Lee, J. Lee, J.S. Park and H.D. Park, "Deep dry etching of borosilicate glass using SF<sub>6</sub> and SF<sub>6</sub>/Ar inductively coupled plasmas", *Microelectronic Engineering*, 82 (2005) 119-128
- [34] A. Goyal, V. Hood and S. Tadigadapa, "High speed anisotropic etching of Pyrex for microsystems applications", *Journal of Non-Crystalline Solids*, 352 (2006) 657-663
- [35] A. Matsutani, M. Hayashi, Y. Morii, K. Nishioka, T. Isonbe, A. Nakajima and S. Matsushita, "SF<sub>6</sub>-based deep reactive ion etching of (001) rutile TiO<sub>2</sub> substrate for photonic crystal structure with wide complete photonic band gap", *Japanese Journal of Applied Physics*, 5 (2012) 098002/1-098002/2
- [36] A.M. Bond, D. Luscombe, K.B. Oldham and C.G. Zoski, "A comparison of the chronoamperometric response at inlaid and recessed disc microelectrodes", *Journal of Electroanalytical Chemistry and Interfacial Electrochemistry*, 249 (1988) 1-14
- [37] N. Godino, X. Borrise, F.X. Munoz, F.J. del Campo and R.G. Compton, "Mass transport to nanoelectrode arrays and limitations of the diffusion domain approach: theory and experiment", *The Journal of Physical Chemistry*, 113 (2009) 11119-11125
- [38] K. Ino, T. Nishijo, T. Arai, Y. Kanno, Y. Takahashi, H. Shiku and T. Matsue, "Local redox-cycling-based electrochemical chip device with deep microwells for evaluation of embryoid bodies", *Angewandte Chemie*, 51 (2012) 6648-6652
- [39] A. Oleinick, F. Zhu, J. Yan, B. Mao, I. Svir and C. Amatore, "Theoretical investigation of generator–collector microwell arrays for improving electroanalytical selectivity: application to selective dopamine detection in the presence of ascorbic acid", *ChemPhysChem*, 14 (2013) 1887-1898

- [40] L. Zhuang, H. Zuo, Z. Wu, Y. Wang, D. Fang and D. Jiang, "Enhanced electrochemical nanoring electrode for analysis of cytosol in single cells", *Analytical Chemistry*, 86 (2014) 11517-11522
- [41] A. Szabo, "Theory of the current at microelectrodes: Application to ring electrodes", *The Journal of Physical Chemistry*, 91 (1987) 3108-3111
- [42] W.E. Morf and N.F. de Rooij, "Performances of amperometric sensors based on multiple microelectrode arrays", *Sensors & Actuators B*, 44 (1997) 538-541
- [43] J. Guo and E. Linder, "Cyclic voltammograms at coplanar and shallow recessed microdisk electrode arrays: guidelines for design and experiment", *Analytical Chemistry*, 81 (2009) 130-138
- [44] F. Sekli-Belaidi, A. Civélas, V. Castagnola, A. Tsopele, L. Mazonq, P. Gros, J. Launay and P. Temple-Boyer, "PEDOT-modified integrated microelectrodes for the detection of ascorbic acid, dopamine and uric acid", *Sensors & Actuators B*, 214 (2015) 1-9
- [45] A. Oleinick, F. Zhu, J. Yan, B. Mao, I. Svir and C. Amatore, "Theoretical investigation of generator-collector microwell arrays for improving electroanalytical selectivity: application to the selective dopamine detection in the presence of ascorbic acid", *ChemPhysChem*, 14 (2013) 1887-1898
- [46] D. Kuzmanova, I.D.C. Jansen, T. Schoenmarker, K. Nazmi, W.J. Teeuw, S. Bizarro, B.G. Loos and U. van der Velden, "Vitamin C in plasma and leucocytes in relation to periodontitis", *Journal of Clinical Periodontology*, 39 (2012) 905-9012
- [47] R.M. Riggin, R.L. Alcorn and P.T. Kissinger, "Liquid Chromatographic method for monitoring therapeutic concentrations of L-dopamine and dopamine in serum", *Clinic Chemistry*, 22 (1976) 782-784

## **Biographies**

Fadhila Sekli Belaïdi was born on February 22 1980. She received the Master's Degree in process and environmental engineering from the French "Institut National des Sciences Appliquées de Toulouse" (France) in 2006. She joined the French "Laboratoire de Génie Chimique" (LGC) from the University of Toulouse (France) in 2007 and received the PhD degree in 2011. Finally, she joined the French "Laboratoire d'Analyse et d'Architecture des Systèmes" from the French "Centre National de la Recherche Scientifique" (LAAS-CNRS) in Toulouse (France) as a postdoctoral fellow. She is working on the development of integrated electrochemical microsensors for chemical and biochemical detection.

Emilie Vanhove graduated in Science and Executive Engineering from the MINES Paris Tech (Ecole des Mines de Paris) in 2006. She joined the CEA (Alternative Energies and Atomic Energy Commission, Paris, France) lab in 2006 and received a PhD in Materials Science in 2009 from the same school. In 2010, she joined the French "Laboratoire d'Analyse et d'Architecture des Systèmes" from the French "Centre National de la Recherche Scientifique" (LAAS-CNRS) in Toulouse (France) as a postdoctoral fellow. Her research interests are focused on the design, modelling, simulation, microfabrication and characterization of integrated electrochemical microsensors.

Matthieu Polverel was born in Bourges (France) on May 26 1992. He joined the French "Laboratoire d'Analyse et d'Architecture des Systèmes" (LAAS) from the French "Centre National de la Recherche Scientifique" (CNRS) in 2014 for an internship. He worked on the physical simulation of microwell arrays with integrated recessed ring nanoelectrodes. He received a Master's degree in biomedical engineering and medical imaging from the French "Ecole Nationale Supérieure de Physique, Electronique, Matériaux" (PHELMMA, INP Grenoble, France) in 2015.

William Tiddi was born in Rome (Italy) in November 1989. He joined the French "Laboratoire d'Analyse et d'Architecture des Systèmes" (LAAS) from the French "Centre National de la Recherche Scientifique" (CNRS) in 2013 for an internship, focusing on multiphysics modelling of detection mechanisms for integrated micro/nanoelectrodes. He received in 2014 the joint Master of Sciences Degree in Nanotechnologies for Information and Communication Technology (NICT) from the Italian "Politecnico di Torino" (Turin, Italy) and the French "Institut polytechnique de Grenoble" (Grenoble, France).

Gabriel Lemerrier was born on 29 December 1990 in Rennes. He obtained a technical degree of electronics and industrial computing in 2010 from the Rennes University (France). He then received the Master's Degree in embedded systems and microsystems in 2014 from the University of Toulouse (France). He finally joined the French "Laboratoire d'Analyse et d'Architecture des Systèmes" from the French "Centre National de la Recherche Scientifique" (LAAS-CNRS) in November 2014 to start a PhD concerning the development of electrochemical micro/nanosensors for the single cell analysis.

Aurélien Lecestre received her Master's Degree in micro/nanomaterials from the French "Université Joseph Fourier" at Grenoble, France, in 2006. She joined the French "Institut d'Electronique, de Microélectronique et de Nanotechnologies" (IEMN) in the frame of a STMicroelectronics collaboration, and received the PhD degree in Material Sciences from the French "Université de Lille 1" in 2009. Then, she worked at the French FEMTO-ST laboratory as an engineer on plasma etching processes during one year, and she did a one year postdoctoral study at Sherbrooke University (Canada) on transistor devices fabrication. In 2012, she joined the French "Laboratoire d'Analyse et d'Architecture des Systèmes" of the French "Centre National de la Recherche Scientifique" (LAAS-CNRS) in Toulouse (France) in the "Techniques and Equipments Applied to Microelectronics" (TEAM) service as engineer. She is working on

the development of plasma etching processes for the manufacturing of integrated micro/nanodevices.

Pascal Dubreuil was born on February 1966. He received the Engineer Degree in physical measurement from the French "Centre National des Arts et Métiers de Toulouse" (CNAM-France) in 2006. He joined the French "Laboratoire d'Analyse et d'Architecture des Systèmes" from the French "Centre National de la Recherche Scientifique" (LAAS-CNRS) in the "Techniques and Equipments Applied to Microelectronics" (TEAM) service as an engineer in 1992. He is working on the development of plasma etching processes for the manufacturing of integrated micro/nanodevices.

Jérôme Launay was born on March 1975. He received the Engineer Degree in electronic engineering from the French "Institut National des Sciences Appliquées de Toulouse" (INSAT-France) in 1998. He joined the French "Laboratoire d'Analyse et d'Architecture des Systèmes" from the French "Centre National de la Recherche Scientifique" (LAAS-CNRS) in 1998 and received the PhD degree from the French "Institut National des Sciences Appliquées de Toulouse" (INSAT-France) in 2001. In 2002, he became lecturer at the French "Université Paul Sabatier de Toulouse" (France). His research activities include the development of chemical microsensors for the detection in liquid phase.

Stéphane Arbault was born in October 1968. He received his PhD in 1996 from University of Paris 7 and the French "Ecole Normale Supérieure de Paris". He was appointed in 1998 as a research associate by the French "Centre National de la Recherche Scientifique" (CNRS). He is currently a senior scientist directing the "Analytical Nanosystems" laboratory of the French "Institute des Sciences Moléculaires" (ISM – university of Bordeaux). He has been working for years on the development of electrochemical microsensors and combined electrochemical-

optical microsystems to monitor secretion processes at single cells and, now, at single organelles, including mitochondria.

Pierre Temple-Boyer was born on October 1966. He received his Engineer Degree in electronic engineering from the Ecole Supérieure d'Electricité (Paris – France) in 1990 and his Master Degree in microelectronics from the French "Université Paul Sabatier de Toulouse" (France) in 1992. He joined the French "Laboratoire d'Analyse et d'Architecture des Systèmes" of the French "Centre National de la Recherche Scientifique" (LAAS-CNRS) in 1992 and received the PhD degree from the French "Institut National des Sciences Appliquées de Toulouse" (France) in 1995. Since then, as a senior researcher, he has been working on the development of analysis micro/nanosystems using silicon-based technologies.

## Table and figure captions

**Table 1.** Experimental conditions for the different ICP-RIE etching processes

**Table 2.** Enhancement of the ring nanoelectrode collection factor according to the step width  $L$  for different microwell inner radii  $R$

**Table 3.** Comparison of experimental (scan rate: 5 mV/s), theoretical and simulated values of limiting currents for recessed ring nanoelectrodes (RNE)

**Table 4.** Selectivity ratios of different electroanalytical systems for the detection of dopamine in presence of ascorbic acid (COMSOL Multiphysics 4.3)

**Figure 1.** Technological process steps: (1,3) Ti/Pt/Ti metallization (lift-off), (2,4) SiO<sub>2</sub> deposition (PECVD), (5) HF etching (opening nanoring contacts), (6) RIE etching (defining rings and disks, opening disk contacts), (a,b,c,d) side view of the microfabricated devices after the different technological steps

**Figure 2.** Scanning electron microscopy (SEM) images of etching micromasking phenomena associated to the formation of CF<sub>x</sub> and/or TiO<sub>x</sub>-based layers (a,b) and their elimination with SF<sub>6</sub> etching chemistry for different microwell radii: (c) 3 μm and (d) 4.5 μm

**Figure 3.** Scanning electron microscopy (SEM) images revealing the upper SiO<sub>2</sub> layer over-etch and the step fabrication ( $L \sim 0.3 \mu\text{m}$ ) on the ring nanoelectrode:

(a) top view of microwell, (b) magnified image of the platinum step,

**Figure 4.** Mass fabrication of recessed ring nanoelectrodes into microwell arrays on a B33 glass substrate: details of (a) a microwell with a recessed ring nanoelectrode, (b,c) a RNE-based arrays and (d) associated electrochemical microsensor

**Figure 5.** Modelling configuration of (a) recessed ring nanoelectrodes integrated into a microwell and (b) associated diffusion profiles using COMSOL Multiphysics 4.3

**Figure 6.** Influences of the main geometrical dimensions on the collection ratio (COMSOL Multiphysics 4.3): (a) total height  $H (= H_1 + T + H_2)$ , (b) inner radius  $R$ , (c) ring nanoelectrode thickness  $T$ , (d) ring nanoelectrode height from the microwell bottom  $H_1$

**Figure 7.** Cyclic voltammograms obtained at different scan rates in 1 mM Fc(MeOH) solution for (a) the 3 $\mu\text{m}$ -radius, platinum disk microelectrode (DME) and (b) the 3 $\mu\text{m}$ -radius, platinum ring nanoelectrodes (RNE): 5 mV/s (red line), 10 mV/s (green line), 50 mV/s (purple line), 100 mV/s (blue line) and 500 mV/s (black line)

**Figure 8.** Cyclic voltammograms obtained at different scan rates in 1 mM Fc(MeOH) solution for 10  $\times$  10, 3 $\mu\text{m}$ -radius, platinum RNE-arrays with different microwell centre-to-centre distances: (a)  $D = 5R$ , (b)  $D = 20R$ : 5 mV/s (red line), 10 mV/s (green line), 50 mV/s (purple line), 100 mV/s (blue line) and 500 mV/s (black line)

**Figure 9.** Chronoamperograms for recessed disk microelectrode (blue curve)

and ring nanoelectrode (red curve) electrode arrays ( $D = 20R$ ,  $R = 3 \mu\text{m}$ ) in 1 mM Fc(MeOH) solution (disk microelectrode and ring nanoelectrode were respectively held at 0.4 V and 0 V versus Ag/AgCl).

**Figure 10.** Cyclic voltammograms at recessed disk microelectrode (scan rate: 50 mV/s) of 1 mM ascorbic acid and dopamine in 0.1M phosphate buffer solution: first experiment (red line) was performed when the ring nanoelectrode was not polarized, second experiment (blue line) when the ring nanoelectrode potential was held at 0.3 V, third experiment (green line) is associated to the oxidation of 1mM of dopamine in 0.1M of phosphate buffer solution.

layers	RIE conditions	etch rate	AZ40XT selectivity
Silicon oxide (SiO <sub>2</sub> )	CF <sub>4</sub> /Ar (40/5 sccm) p = 4 mTorr P <sub>icp</sub> = 500 W, P <sub>bias</sub> = 40 W	150 nm/min	0.72
Titanium (Ti) / titanium oxide (TiO <sub>x</sub> )	SF <sub>6</sub> (50 sccm) p = 10 mTorr P <sub>icp</sub> = 500 W, P <sub>bias</sub> = 40 W	4 nm/min	0.015
Platinum (Pt)	Cl <sub>2</sub> (20 sccm) p = 3 mTorr P <sub>icp</sub> = 78 W, P <sub>bias</sub> = 3 W	17 nm/min	0.34

**Table 1.** Experimental conditions for the different ICP-RIE etching processes

<i>L</i> width ( $\mu\text{m}$ )	collection ratio (%)		
	<i>R</i> = 1.5 $\mu\text{m}$	<i>R</i> = 3 $\mu\text{m}$	<i>R</i> = 4.5 $\mu\text{m}$
0	87.7	78.0	70.4
0.1	89.8	81.2	74.1
0.2	90.6	82.4	75.7
0.3	91.1	83.3	76.7
0.4	91.5	83.9	77.7
0.5	91.8	84.5	78.6

**Table 2.** Enhancement of the ring nanoelectrode collection factor according to the step width *L* for different microwell inner radii *R*

inner radius $R$ ( $\mu\text{m}$ )	limiting current $I_{lim}$ (pA) for a scan rate of 5 mV/s		
	experimental	theoretical model	COMSOL simulation
3	400	380	390
4.5	650	660	620

**Table 3.** Comparison of experimental (scan rate: 5 mV/s), theoretical and simulated values of limiting currents for recessed ring nanoelectrodes (RNE).

electroanalytical system configuration	$[AA]/[Dop]$ ratio	dopamine versus ascorbic acid selectivity ratio (%)		
		$R = 1.5 \mu\text{m}$	$R = 3 \mu\text{m}$	$R = 4.5 \mu\text{m}$
proposed DME-RNE system [this work]	1	87.4	75.8	69.3
	10	40.9	24.0	18.4
	100	6.5	3.1	2.2
recessed DME array with top plane electrode [45]	1	97.5	97.0	96.0
	10	79.7	76.5	70.7
	100	28.1	24.5	19.5

**Table 4.** Selectivity ratios of different electroanalytical systems for the detection of dopamine in presence of ascorbic acid (COMSOL Multiphysics 4.3)

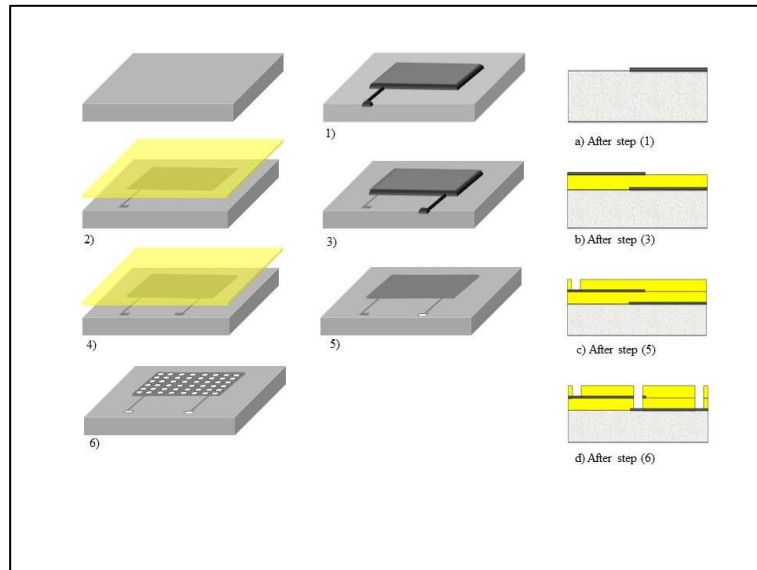


**Figure 1.** Technological process steps: (1,3) Ti/Pt/Ti metallization (lift-off), (2,4) SiO<sub>2</sub> deposition (PECVD), (5) HF etching (opening nanoring contacts), (6) RIE etching (defining rings and disks, opening disk contacts), (a,b,c,d) side view of the microfabricated devices after the different technological steps

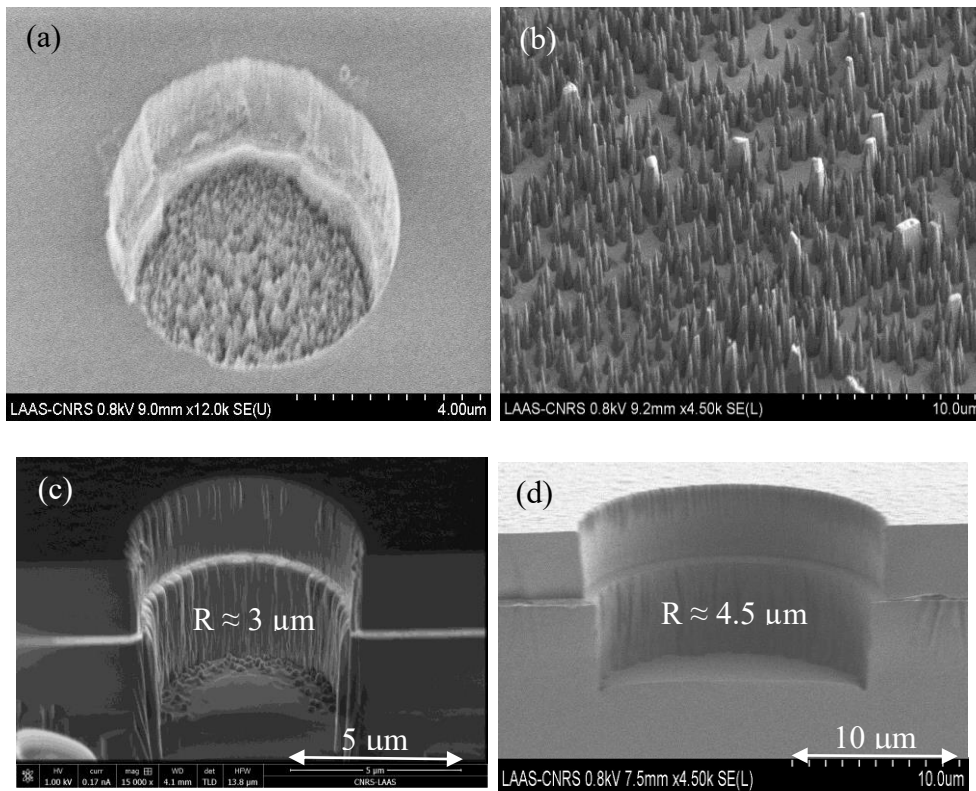


**Figure 2.** Scanning electron microscopy (SEM) images of etching micromasking phenomena associated to the formation of  $\text{CF}_x$  and/or  $\text{TiO}_x$ -based layers (a,b) and their elimination with  $\text{SF}_6$  etching chemistry for different microwell radii: (c)  $3 \mu\text{m}$  and (d)  $4.5 \mu\text{m}$

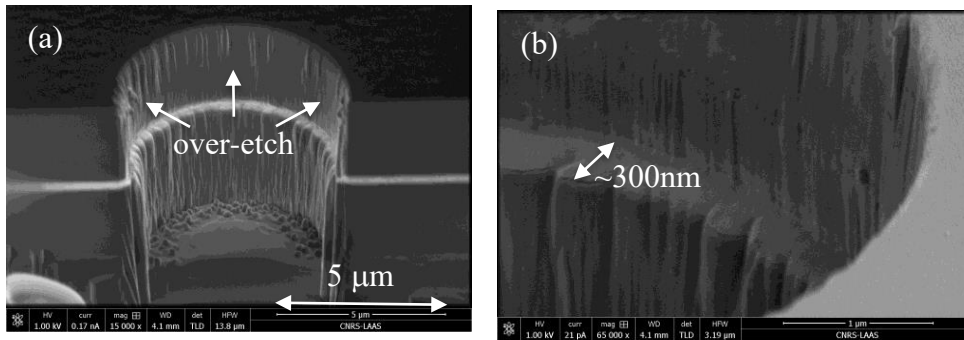


**Figure 3.** Scanning electron microscopy (SEM) images revealing the upper SiO<sub>2</sub> layer over-etch and the step fabrication ( $L \sim 0.3 \mu\text{m}$ ) on the ring nanoelectrode:

(a) top view of microwell, (b) magnified image of the platinum step,

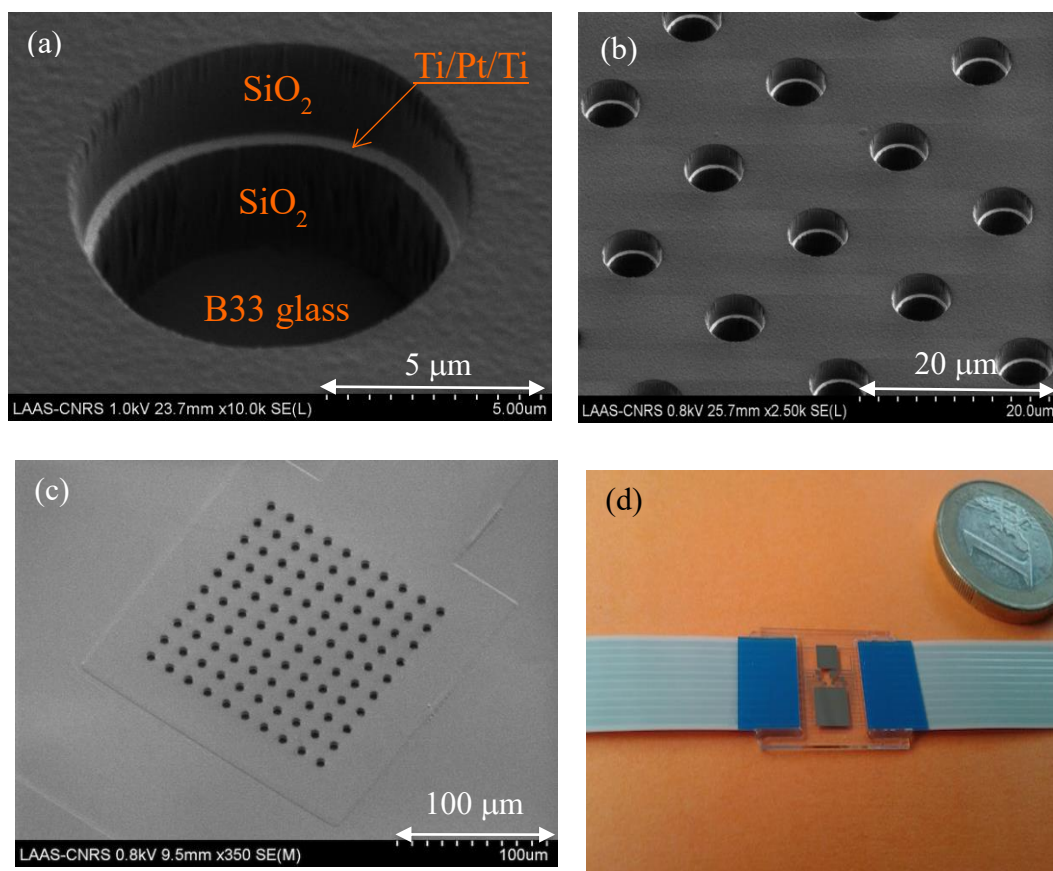


**Figure 4.** Mass fabrication of recessed ring nanoelectrodes into microwell arrays on a B33 glass substrate: details of (a) a microwell with a recessed ring nanoelectrode, (b,c) a RNE-based arrays and (d) associated electrochemical microsensor

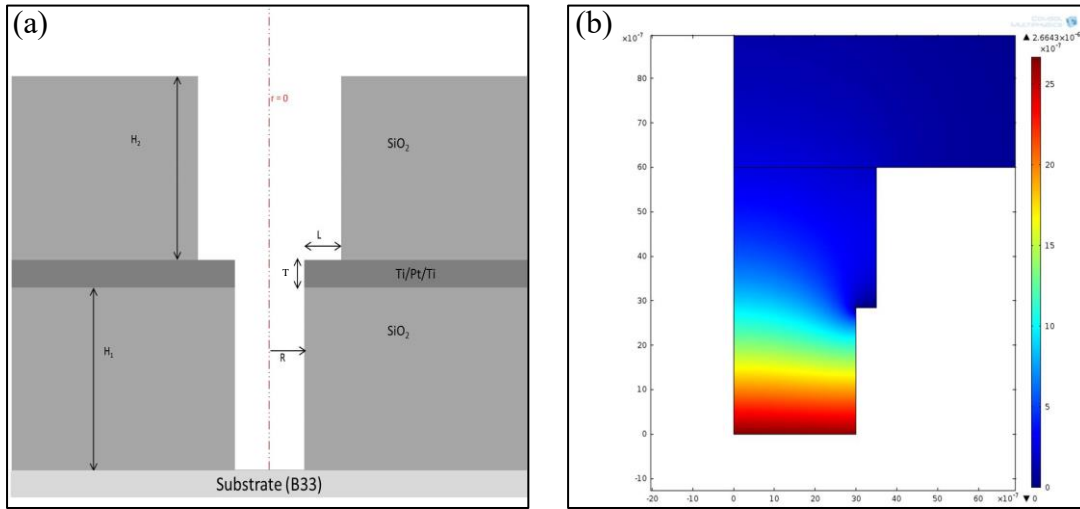


**Figure 5.** Modelling configuration of (a) recessed ring nanoelectrodes integrated into a microwell and (b) associated diffusion profiles using COMSOL Multiphysics 4.3

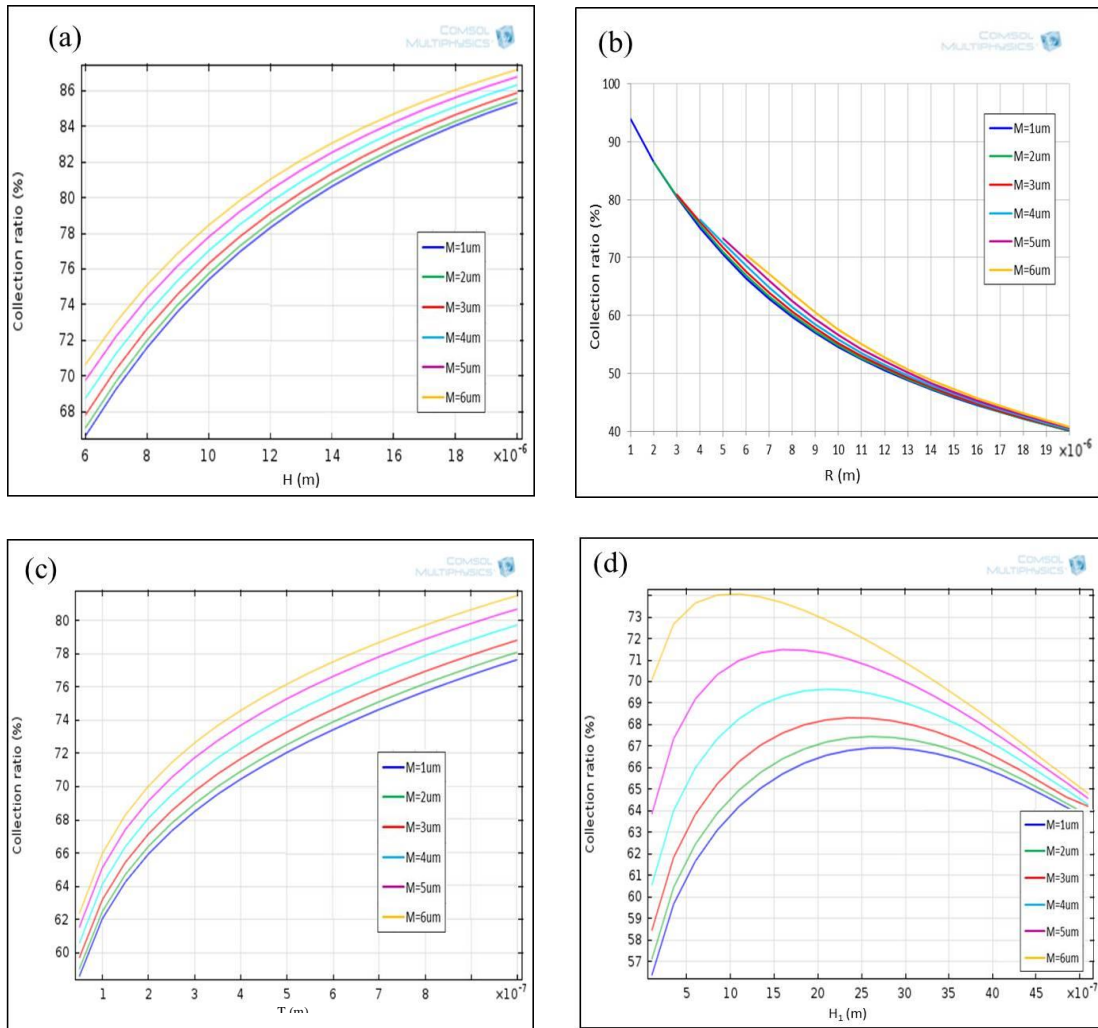


**Figure 6.** Influences of the main geometrical dimensions on the collection ratio

(COMSOL Multiphysics 4.3): (a) total height  $H$  ( $= H_1 + T + H_2$ ), (b) inner radius  $R$ ,

(c) ring nanoelectrode thickness  $T$ , (d) ring nanoelectrode height from the microwell bottom  $H_1$

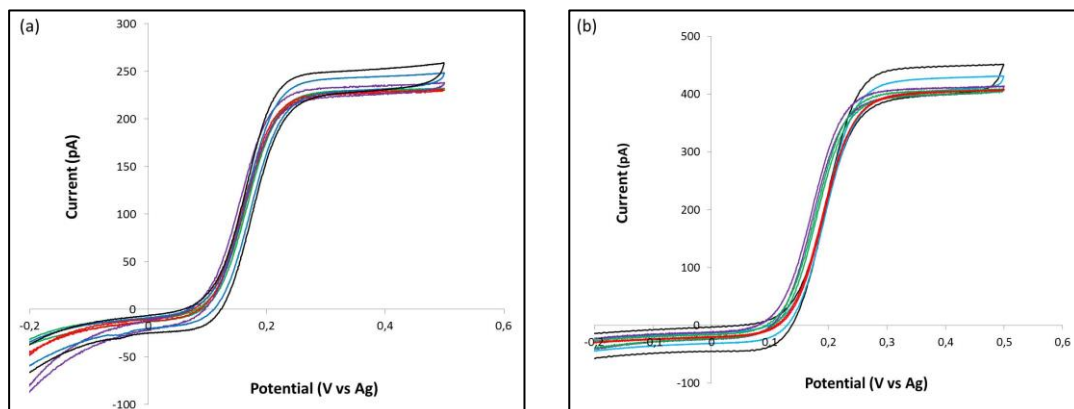


**Figure 7.** Cyclic voltammograms obtained at different scan rates in 1 mM Fc(MeOH) solution for (a) the 3 $\mu$ m-radius, platinum disk microelectrode (DME) and (b) the 3 $\mu$ m-radius, platinum ring nanoelectrodes (RNE): 5 mV/s (red line), 10 mV/s (green line), 50 mV/s (purple line), 100 mV/s (blue line) and 500 mV/s (black line)

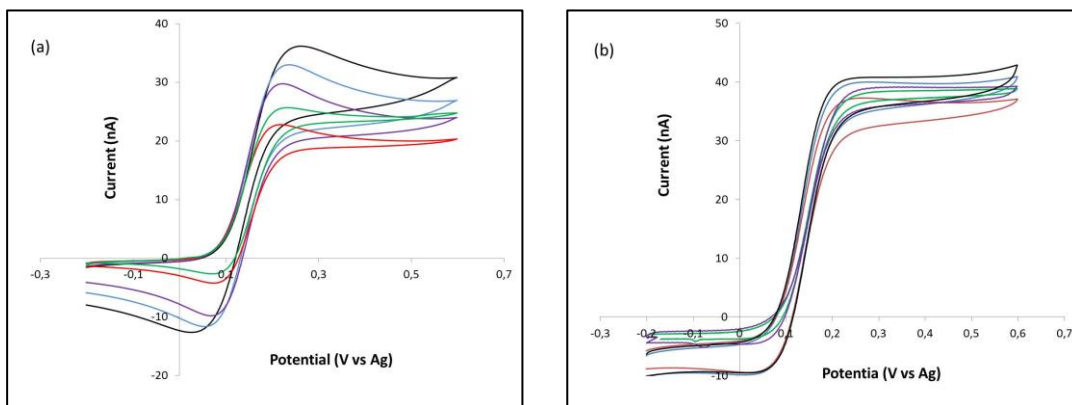


**Figure 8.** Cyclic voltammograms obtained at different scan rates in 1 mM Fc(MeOH) solution for  $10 \times 10$ ,  $3\mu\text{m}$ -radius, platinum RNE-arrays with different microwell centre-to-centre distances: (a)  $D = 5R$ , (b)  $D = 20R$ : 5 mV/s (red line), 10 mV/s (green line), 50 mV/s (purple line), 100 mV/s (blue line) and 500 mV/s (black line)

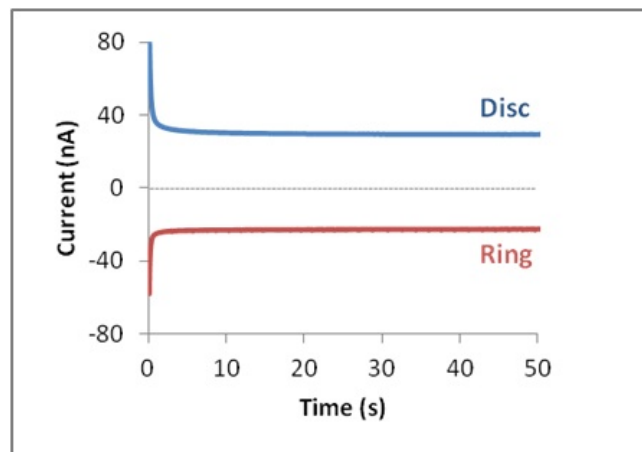


**Figure 9.** Chronoamperograms for recessed disk microelectrode (blue curve) and ring nanoelectrode (red curve) electrode arrays ( $D = 20R$ ,  $R = 3 \mu\text{m}$ ) in 1 mM Fc(MeOH) solution (disk microelectrode and ring nanoelectrode were respectively held at 0.4 V and 0 V versus Ag/AgCl).

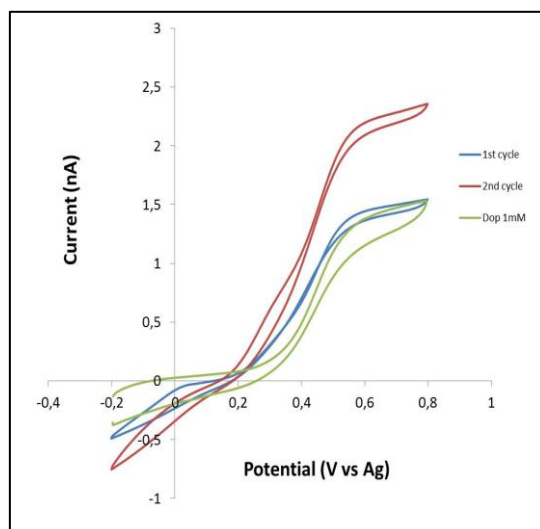


**Figure 10.** Cyclic voltammograms at recessed disk microelectrode (scan rate: 50 mV/s) of 1 mM ascorbic acid and dopamine in 0.1M phosphate buffer solution: first experiment (red line) was performed when the ring nanoelectrode was not polarized, second experiment (blue line) when the ring nanoelectrode potential was held at 0.3 V, third experiment (green line) is associated to the oxidation of 1mM of dopamine in 0.1M of phosphate buffer solution.